Catalysis Science & Technology

Accepted Manuscript

This article can be cited before page numbers have been issued, to do this please use: M. N. N. Shaikh, A. N. Kalanthoden, A. Helal, Md. A. Aziz, M. Bououdina and A. Syed, *Catal. Sci. Technol.*, 2018, DOI: 10.1039/C8CY00936H.

ROYAL SOCIETY OF CHEMISTRY

rsc.li/catalysis

DOI: 10.1039/C8CY00936H

Journal Name

ARTICLE

Facile hydrogenation of *N*-heteroarenes by magnetic nanoparticles supported sub-nanometric Rh catalysts in aqueous medium

Received 00th January 20xx,
Accepted 00th January 20xx

DOI: 10.1039/x0xx00000x

www.rsc.org/

M. Nasiruzzaman Shaikh,*[,a] Md. Abdul Aziz,[a] Abdul Nasar Kalanthoden,[b] Aasif Helal,[a] Abbas S. Hakeem,[a] and Mohamed Bououdina[c]

The hydrogenation of nitrogen-containing heterocyclic precursors in aqueous medium at low temperature without imposing molecular hydrogen pressure, is quite challenging. Herein, we report the synthesis and performance of a novel catalyst capable of facile hydrogenation (employing tetrahydroxydiboron (THDB) as the reductant) of *N*-heteroarenes in water at 80 °C with good recyclability. Rhodium particles in the sub-nano region (< 1 nm) were produced by *in-situ* reduction of a Rh precursor on freshly prepared superparamagnetic iron oxide nanoparticles (SPIONs, Fe_3O_4), using aqueous ammonia as reducing agent at 50 °C. HRTEM images and elemental mapping reveal homogenous distribution of < 1 nm Rh particles within the matrix of Fe_3O_4 nanoparticles having average size was within a narrow range of 7-9 nm. The superparamagnetic nature of the composite was confirmed by VSM analysis. The Rh@Fe_3O_4 catalyst was found to be highly efficient in the heterogeneous hydrogenation of nitrogen-containing heterocyclic compounds with quantitative conversion. It showed selectivity towards the hydrogenation of 1,2,3,4-tetrahydroquinoline (py-THQ) in water using THDB with high TOF of 1632 h^{-1}. These results are compared with the conversion and selectivity data obtained from the reduction by molecular hydrogen gas pressure. The catalytic activity is extended to the successful hydrogenation of simple aromatics like benzene, toluene etc. Isotopic labelling studies were performed to know the source of hydrogen in quinoline hydrogenation in presence of THDB. It was found that it could be used for 16 consecutive cycles with gaseous hydrogen, without any undesired byproducts; it also retained its original crystallinity.

Introduction

Catalytic hydrogenation of organic functional groups, such as alkene[1-3], alkyne[4], carbonyl[5], imine[6], nitro[7-9] etc., has recently become very crucial in organic synthesis. For example, the direct hydrogenation of *N*-bearing heterocyclic compounds, such as quinoline, to 1,2,3,4- tetrahydroquinoline (py-THQ)[10] has attracted lot of interest due to their great relevance as major building blocks in the synthesis of agrochemicals, pharmaceuticals, dyes, alkaloids and numerous other fine products.[11] However, the heteroarene hydrogenation encounters serious challenges owing to their rather high stability; the lability of the lone-pair of electrons on the heteroatom (nitrogen) often deactivates the catalysts.[12] Hydrogenation of quinoline may produce three possible products, such as, py-THQ, 5,6,7,8- tetrahydroquinoline (bz-THQ) and decahydroquinoline (DHQ) in different or the same ratio. The underlying challenge, therefore, is to generate the hydrogenated pyridine ring compound (py-THQ) selectively as the prime product. In this context, Ru[13], Rh[14], Ir[15] and Pd[16] based homogeneous catalysts have been applied for the direct hydrogenation of quinoline with excellent results. For example, Fish and co-worker reported Rh-based catalyst (η^5 -pentamethylcyclopentadienyl) rhodium dicationic complex, $[Cp^*Rh(CH_3CN)_2]^{2+}$ for the regioselective reduction of nitrogen-containing model compounds such as quinoline.[17-19] Recently, an iridium complex of BINOL-derived phosphoramidite PipPhos was used for the hydrogenation of a series of quinolines.[20] Unfortunately, these homogeneous catalytic procedures suffer from serious drawbacks of employing harsh reaction conditions accompanied by highly tedious and cumbersome purification process.[20] Their rather low efficiency limits and restricted reusability options pose impediments to wide commercialization endeavours.

Recent focus on the development of recyclable and more efficient catalysts has drawn attention to their production in a greener and safer environment. Therefore, alternative to homogeneous catalysis is required where separation of the product is expected to be effortless with high product purity. Hence, the path of heterogeneous catalysis becomes an

[a] *Center of Research Excellence in Nanotechnology (CENT), King Fahd University of Petroleum and Minerals, Dhahran-31261, Saudi Arabia. Email: mnshaikh@kfupm.edu.sa*
[b] *King Fahd University of Petroleum and Minerals, Dhahran-31261, Saudi Arabia*
[c] *Dept. of Physics, University of Bahrain, Kingdom of Bahrain*
† Footnotes relating to the title and/or authors should appear here.
Electronic Supplementary Information (ESI) available: [details of any supplementary information available should be included here]. See DOI: 10.1039/x0xx00000x

View Article Online
DOI: 10.1039/C8CY00936H

obvious choice.[21-23] Accordingly, numerous heterogeneous catalytic systems based on Mn[24], Ni[25], Ru[26-28], Rh[29-32], Ir[33], Pt[34], Pd[35-37] and Au[38,39] have been developed for quinoline hydrogenation. Although, in some cases complete conversion of quinoline with good selectivity was observed with 50 bar or more of H_2 pressure at about 200 °C, the reaction, nevertheless, progressed at much slower pace, taking tens of hours to reach to completion; it also involved the use of toxic organic solvents. Thus, there is a need to seek alternative material paths, where the reactions could be conducted in low temperature regimes without employing hydrogen gas at high pressure in a green medium such as water. In this context, judicious choice of the solid support is crucial to obtain high conversion, greater selectivity and reusability. A number of precious metal-impregnated solid supports such as zeolite, polymer, silica and cellulose have been investigated as catalytic systems.[21-39] However, ligand-free metal supported on SPIONs has rarely been explored. It should be stated that solid-supported catalyst

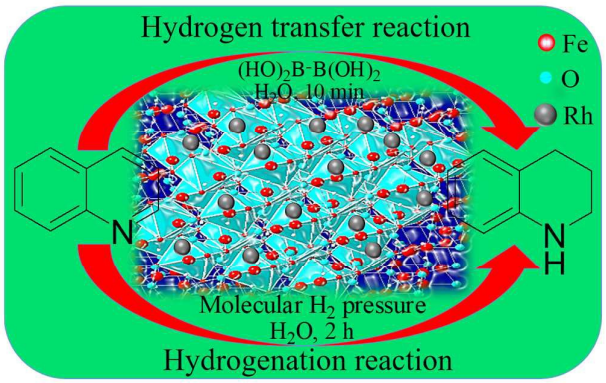

Fig.1 Schematic representation of quinoline hydrogenation using catalyst, Rh@Fe_3O_4, and THDB as reductant in water.

require post-reaction separation from the products; this is generally achieved either by filtration, centrifugation or precipitation, each of which severely affects the prospects of reusability as a result of gradual but monotonous loss of material in every cycle.[40]

Superparamagnetic iron oxide nanoparticles (SPIONs) have attracted a great deal of attention because of their straightforward synthesis procedure from low cost precursors. Their insolubility in water (and other common solvents) and distinct magnetic attributes render their separation from the product stream by an external magnet effortless. Magnetically separable catalysts have been exploited to synthesize biphenyl,[41] higher olefins,[42] asymmetric hydrogenated ketones[43] and transesterified biodiesel.[44] No magnetic catalyst has, however, been developed for agile and highly selective hydrogenation of *N*-heterocyles in water without applying molecular hydrogen pressure.

As a part of our sustained efforts towards developing highly active and reusable noble-metal supported solid catalysts,[45-46] in this study we describe a new construct consisting of sub-nanometer rhodium nanoparticles supported on ultra-small magnetic nanoparticles. Magnetite (Fe_3O_4) was chosen as support because of its simple, easy and cost-effective synthesis from inexpensive precursors and its proven magnetic properties. Moreover, the reaction could be carried out in water – a benign and green solvent. For the first time, tetrahydroxydiboron was employed for reduction of quinoline thus obviating the need for using compressed hydrogen gas. The availability of basic sites of the solid-support (Fe_3O_4) to attract the substrate and interaction with Rh nanoparticles appear favourable for high catalytic activity and exceptional reusability without deactivation.

Experimental

Materials. All chemicals were purchased from Sigma-Aldrich and were used as-received unless otherwise stated. Standard procedures were followed for the dry and deoxygenated solvents. Schlenk line techniques were used to carry out reactions under inert atmosphere wherever needed. Deionized (DI) water (specific conductivity: 18.2 mΩ) was used in all the experiments.

FTIR. Furrier-Transform Infrared (FTIR) spectroscopic data were obtained on a Nicolet 720 in the wave number range of 500 to 4000 cm^{-1}, using KBr as the IR transparent window material.

XRD. X-ray diffraction data were collected on Rigaku model Ultima-IV diffractometer employing Cu-Kα radiation (λ = 1.5405 Å) at 40 kV and 25 mA over a 2θ range between 20 and 90°.

TEM. The Transmission Electron Microscopy images were acquired at the Instituto de Nanociencia de Aragón (LMA-INA), University of Zaragoza, Spain, on a TEM (JEOL, JEM 2011) operated at 200 kV with 4k × 4k CCD camera (Ultra Scan 400SP, Gatan). The TEM samples were prepared by dropping on a copper grid from an ethanolic suspension and drying at room temperature.

DLS: The particle size was determined by the Microtrac nanosize analyzer (Model S3500/Turbotrac, USA). Powder samples were taken in ethanol and sonicated using ultrasonic probe sonicator (Model VC 50, Sonics, USA) for 1 h to have maximum deagglomeration. The particle size was determined on average based on five measurements.

ICP-OES. The amount of Rh in the catalyst was determined by Inductively Coupled Optical Emission Spectrometry (ICP-OES; PlasmaQuant PO 9000 - Analytik Jena**)**. The samples were first digested in a dilute HNO_3 and HCl mixture. Calibration curves were prepared for Rh and Fe using standard solutions (ICP Element Standard solutions, Merck).

View Article Online
DOI: 10.1039/C8CY00936H

SEM-EDS. Samples for Scanning Electron Microscopy (SEM) were prepared from ethanolic suspensions on alumina stubs and coated with gold in an automatic gold coater (Quorum, Q150T E). For the elemental analysis and mapping, the energy dispersive X-ray spectra (EDS) were collected on a Lyra 3 attachment to the SEM.
VSM. The magnetic susceptibilities were measured at room temperature using a vibrating sample magnetometer (VSM, model PMC Micromag 3900) equipped with a 1 tesla magnet.

Autoclave. Catalytic reactions were performed in Teflon lined autoclaves from HiTech, USA (model M010SSG0010-E129A-00022-1D1101), fitted with a pressure gauge and a mechanical stirrer.

GC-MS: Catalytic products were identified by a Shimadzu 2010 Plus (Japan) gas chromatograph attached with a mass spectrometer. The disappearance of the reactant and sequential appearance of the product was recorded in real-time, identifying the species in terms of their molecular ion (M^+) by comparing and matching them with the available Willey library of the mass spectrum database, in addition to the identification of mass fragmentation.

NMR: Solution ^{1}H and ^{13}C NMR experiments were performed on a Bruker Ascend 400 spectrometer at Saudi International Petrochemical Company (SIPCHEM) in Dhahran Techno Valley (DTV) and chemical shifts (δ) values were referenced to tetramethylsilane (TMS) as an internal standard.

Synthesis of Rh@Fe_3O_4 Catalyst. Magnetite (Fe_3O_4) nanoparticles in the range of 7-9 nm were prepared according to a procedure described elsewhere.[47,48] Nanoscale Fe_3O_4 powder (200 mg) was suspended in dry methanol (30 mL) and sonicated for 3 h. 200 μL of rhodium (III) nitrate solution (1.9 x10^{-4} mol, 0.019 g of Rh) was added to the homogeneous suspension of magnetite and stirred at 50 °C for 3 h under argon atmosphere. Concentrated NH_4OH (27 M) was added to achieve and maintain a pH >12, standing the mixture for 4 h. Particles were settled down by means of an external magnet. They were washed with a copious amount of water followed by dichloromethane.

Quinoline hydrogenation with THDB. The catalytic hydrogenation of quinoline was performed in a parallel 10-place reaction tube reactor fitted with a magnetic stirrer and a Teflon stopper. To the Rh@Fe_3O_4 (2 mg) suspension in DI water (2 mL), quinoline (0.5 mmol, 0.65 μL) was added and the system flushed with argon gas 3 times. Tetrahydroxydiboron (4 mmol) was added, capped with Teflon stopper and heated to 80 °C. The reaction progress was monitored by TLC (thin layer chromatography); the product was extracted with ethyl acetate (EA) and dried with sodium sulphate. It was passed through a short silica gel column using EA and hexane (8:2) mixture as an eluent. Conversion was measured by GC and identified by the GC-MS.

***N*-heteroarene hydrogenation with gaseous hydrogen.** For this, the catalyst (5 mg) and the selected reactant (for example, pyridine, 0.5 mL) mixture was placed in a Teflon-lined autoclave fitted with a pressure gauge, mechanical stirring and automatic temperature controller. The reactor was flushed repeatedly with H_2, filled with H_2 up to the 40 bar, and the reaction initiated with heating and stirring and continued for 10 h. After the completion of reaction, the reactor was allowed to cool down to room temperature, depressurized and opened. The degree of conversion measured in a GC and the product was identified by the NMR or GC-MS.

Aromatic hydrogenation with gaseous hydrogen. The similar method was followed for the hydrogenation of aromatic compounds like benzene, toluene and xylene.

Results and discussion

Synthesis and characterization

The novel catalyst was prepared by the deposition of Rh precursors on the surface of magnetite (Fe_3O_4) support(average particle size ≈7-9 nm) followed by mild reduction using ammonia to make sure no more unreacted Rh precursors in the reaction system.

Structural characterization of the catalyst was carried out by a number of analytical and spectroscopic techniques. The phase analysis was investigated by X-ray diffractometry and comparative XRD signatures of magnetite powder with and without Rh are shown in Fig. 2. Well-defined broad peaks with relatively high intensity are observed, indicating high crystallinity with spinel structure of the freshly prepared Fe_3O_4 and Rh@Fe_3O_4 nanopowders.

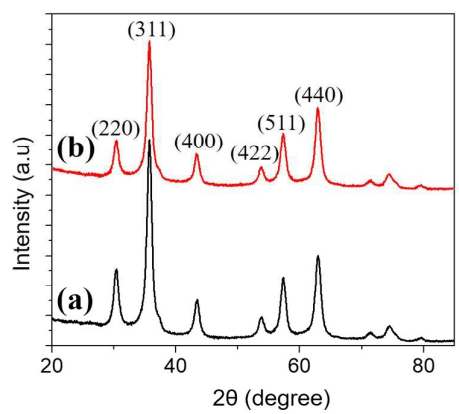

Fig. 2 XRD spectra of (a) pure Fe_3O_4 and (b) Rh@Fe_3O_4.

Furthermore, the superimposition with the pure Fe_3O_4 peaks indicates the preservation of Fe_3O_4 structural lattice arrangement upon decoration of sub-nanosized Rh. XRD angle at (2θ) 30.22°, 35.70°, 43.10°, 53.40°, 57.10° and 63.20° demonstrated the purity and formation of single phase nanomaterials with cubic structure (JCPDS card No. 01-075-

View Article Online
DOI: 10.1039/C8CY00936H

0449) of magnetite (Fe_3O_4).[49] It is worthy to note that no additional recognizable peak(s) attributed to Rh was detected within the measured range of diffraction pattern. This may be attributed to the low concentration(s) as well as sub-nanometer sized Rh particles are dispersed over the spherical solid surface of magnetite and hence it is hard to detect in XRD.

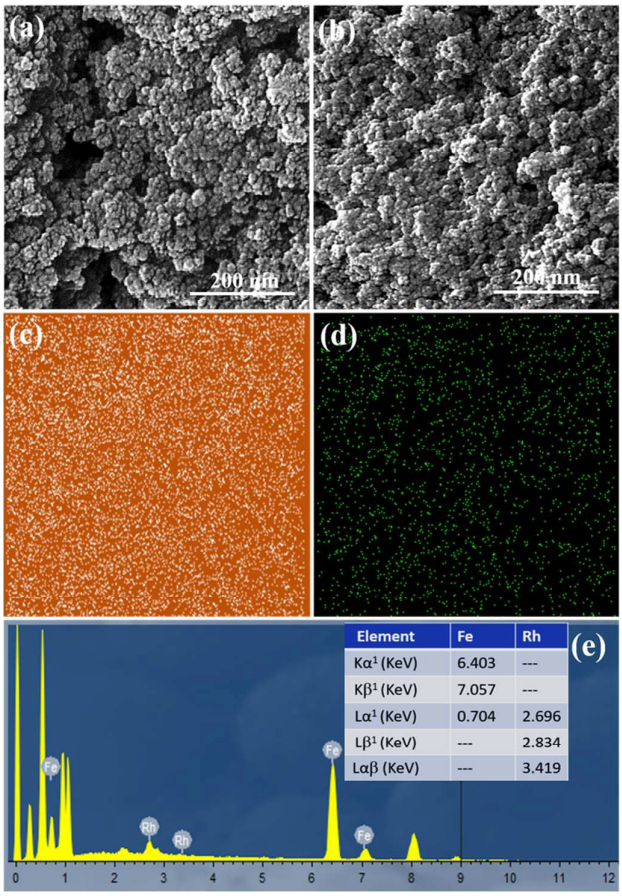

Element	Fe	Rh
Kα¹ (KeV)	6.403	---
Kβ¹ (KeV)	7.057	---
Lα¹ (KeV)	0.704	2.696
Lβ¹ (KeV)	---	2.834
Lαβ (KeV)	---	3.419

Fig. 3 SEM image of (a) Fe_3O_4 and (b) Rh@Fe_3O_4; Elemental mapping of (c) Fe_3O_4 and (d) Rh@Fe_3O_4; (e) SEM-EDS of Rh@Fe_3O_4.

The size of magnetite crystallites was estimated to be less than 10 nm from Debye-Scherrer equation; this was also validated from the FESEM and TEM images of the catalyst specimen (Fig. 3 and 4). The structural refinement performed by using the Rietveld method (*see supporting information*, Table 1) which confirmed the formation of the desired phase in high purity with a goodness of fit close to the unity (GoF = 1.07-1.13). This suggests that the incorporation of Rh did not alter the structure nor dilate the lattice of the parent support, suggesting that SPIONs remained stable during the Rh decoration process.

The morphological and nanostructural features of Fe_3O_4 and Rh@Fe_3O_4 particles were investigated by scanning electron microscope (SEM) and transmission electron microscopy (TEM), which revealed the formation of well-dispersed spherical particles, about 7-9 nm in size with narrow size distribution (Fig. 3a-e and 4a-g), which was confirmed by measurement with a particle size analyzer (Fig 4d). Furthermore, the surface of magnetite nanoparticles (7-9 nm; Fig. 4a) is uniformly decorated with Rh particles that are < 1 nm in size (Fig. 4b); as corroborated by the confined area of elemental mapping (Fig 3c-d). It is speculated that during the process of decoration on magnetite nanoparticles, increase in surface potential led to the decrease in the size of Rh particles to the sub-nano region.[50,51] Scanning tunnelling electron microscopy (STEM) was used to investigate the local physical and electronic structure of surfaces, which led to the identification of Rh in the sample (Fig 3e, 4e and *see supporting information, Fig S1*). HRTEM image (Fig. 4f) confirms the high crystallinity of Fe_3O_4 nanoparticles, which was also concluded from the powder XRD pattern shown earlier in Fig. 2. Figure 4f and the Bragg reflections in the corresponding SAED pattern (Fig. 4g) yielded a *d*-value of 0.249 nm which could be assigned to the <311> reflection of magnetite in the specimen in cubic crystal structure. However, ICP-OES data demonstrates that the ratio of Fe/Rh is found to be 94:6 which is further confirmed by both EDS studies coupled with both SEM and TEM. FTIR of Rh@Fe_3O_4 showed a vibrational red shift of 3 cm^{-1} from 581 cm^{-1} for the Fe-O bond in the parent magnetite and these results demonstrated that after incorporation of Rh nanoparticles on magnetite surface did not significantly affect Fe-O vibration.

The XPS studies have been carried out to know the composition and oxidation states of the element used in the process. The XPS data revealed the formation of Rh^0 on the surface of Fe_3O_4, as corroborated by the peaks with binding energies of 307.1 eV ($3d_{5/2}$) and 311.8 eV ($3d_{3/2}$) associated with Rh^0 species.[52] A small shoulders at the photoelectron energy of 308.9 eV corresponding to Rh_2O_3 was also seen, which could be an artifact of Rh oxidation by ambient air.[52]

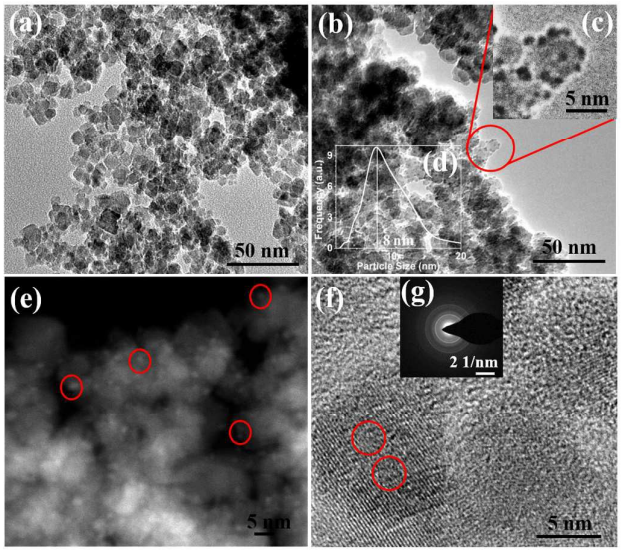

View Article Online
DOI: 10.1039/C8CY00936H

Fig. 4 TEM images of: (a) Fe_3O_4, and (b) Rh@Fe_3O_4. Insets (c) shows magnified image of RhNPs decorated on the Fe_3O_4 particles and (d) particle size distribution curve of Rh@Fe_3O_4. The STEM image of Rh@Fe_3O_4 particles is shown in (e); red circles denote RhNPs (size: < 1 nm). The HRTEM image of Rh@Fe_3O_4 is shown in (f); inset (g) shows the selected area electron diffraction (SAED) pattern of Fe_3O_4 on Rh@Fe_3O_4; red circles denote RhNPs (size: < 1 nm).

The magnetization (M) vs. applied magnetic field (H) curves measurements were conducted by vibrating sample magnetometery at room temperature. As can be seen in figure 5a, both Fe_3O_4 and Rh@Fe_3O_4 show superparamagnetic behaviour as no hysteresis loop was found in the recorded curve. It is important to highlight that slight reduction of saturation magnetization establishes the viability of the surface decoration with non-magnetic element, Rh.

From the foregoing discussion, it is clear that the reported preparation technique offers an excellent pathway to designing catalysts with well-dispersed, sub-nanometre Rh particles dispersed on nanostructured magnetic support; this recipe could be easily extended to other solid surfaces as well, for important organic transformations, including the hydrogenation of aromatic precursors.

Catalysis

Hydrogen transfer reaction of quinoline using tetrahydroxydiboron (THDB) as reductant

To evaluate the selectivity and conversion, quinoline was used a model benchmark substrate for the catalytic hydrogen transfer reactions using Rh@Fe_3O_4 as catalyst. Efficacy of the magnetic catalyst towards hydrogenation was tested by using THDB as the reductant in lieu of compressed H_2 gas in cylinders. No conversion of py-THQ was observed in presence of the catalyst, Rh@Fe_3O_4, in absence of THDB. In presence of THDB without catalyst, the reaction was proceeded in much slower rate and after 10 min of the reaction, 27% conversion was observed (table 1, entry# 1). Hence, a combination of Rh@Fe_3O_4 and THDB, as hydrogen source, is required to carry out the reduction process. Table 1 summarizes the experimental parameters and the results of quinoline hydrogenation in various media.

Table 1. Rh@Fe_3O_4-mediated hydrogenation of quinoline[a] using THDB

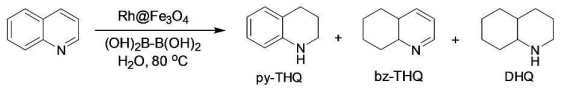

Entry	Solvent	Temp (°C)	Time (min.)	Conv.[b] (%)	Sel.[c] (%)	TOF (h^{-1})
1	Water	rt	30	---	---	---
		50	10	88	100	1436
			20	94	100	765
		60	10	92	100	1501
		60[d]	10	27	nd	---
		80	10	> 99	100	1632
2	IPA	80	10	15	100	245
			60	67	100	182
			300	94	100	51
3	THF	80	300	---	---	---
4	Cyclohexane	80	300	---	---	---
5	Methanol	80	300	nd	nd	---
6	1,4-dioxane	80	300	---	---	---

[a]2 mg catalyst, 0.5 mmol of quinoline and 4 mmol of THDB in 2 mL water were used; [b]measured by GC; [c]selectivity towards py-THQ, identified by GC-MS and NMR; [d]without catalyst but with THDB; rt: room temperature; nd: not determined.

To explore the catalytic hydrogenation activity, we selected the benchmark substrate quinoline as a model reaction and its degree of sensitivity towards hydrogenation was tested (Table 1). Samples were taken out periodically and analysed by thin layer chromatography (TLC), gas chromatography (GC) and gas chromatography-mass spectrometry(GC-MS) to evaluate conversion and selectivity; this assisted in optimizing the reaction process parameters such as, the solvent, time and temperature, amount of catalyst and the reactant and, hydrogen precursor. Since, the activity and selectivity was an artefact of the solvent selection, the hydrogenation was carried out in a number of solvents, such as, IPA, THF, cyclohexane, methanol and 1,4-dioxane, as summarized in Table 1. No hydrogenation occurred in methanol, dioxane, cyclohexane or THF even after long reaction time (Entry # 3-6). In addition, the reaction progress in IPA was quite slow and did not reach completion even after prolonging the reaction time to 5 h. On the other hand, the conversion was quantitative in water. The effect of temperature was also briefly examined. There was no conversion at room temperature, but the conversion was appreciable at 50 and 80 °C (table 1, entry# 1). In fact, it took only 10 min. at 80 °C to achieve > 99% conversion with 100% selectivity with the TOF value of 1632 h^{-1}. Nevertheless, on increasing the reaction temperature, no deteriorating effect on selectivity was evident from the results (table 1, entry# 1). The effect of relative concentration of THDB on quinoline hydrogenation in water as a function of on-stream reaction time, is shown in Table 2. The amount of THDB were varied systematically from 2 to 8 equivalent of quinoline. The conversion was seen to increase steadily with increasing THDB and 97% conversion into py-THQ was achieved with 6 equivalent THDB after 20 min. of reaction time. But the optimum conversion of > 99% was achieved with 8 equivalent of THDB (table 2, entry # 4) in just 10 min with very high TOF value, 1632 h^{-1}. Hence, quinoline can be smoothly hydrogenated to py-THQ in water at 80 °C by adding eight equivalent of THDB as hydrogen source to selectively produce py-THQ in 10 minutes. It should be also pointed out that in a conventional scheme of quinoline hydrogenation, bz-THQ and DHQ have also been observed.[31]

Table 2. Effect of the relative concentration of tetrahydroxydiboron (THDB) on quinoline[a] hydrogenation in water as a function of on-

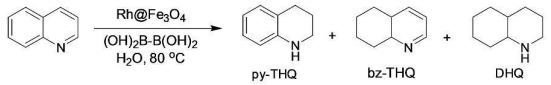

Entry	THDB (mmol)	Time (min)	Conv.[b] (%)	Sel.[c] (%)	TOF (h^{-1})
1	2	30	64	100	347
2	4	30	93	100	504
3	6	20	97	100	789
4	8	10	>99	100	1632

[a]substrate 1 mmol and 2 mg catalyst; [b]measured by GC; [c]selectivity towards py-THQ, identified by GC-MS and NMR.

View Article Online
DOI: 10.1039/C8CY00936H

stream reaction time

The hydrogenation of heterocyclic rings in comparison to carbocyclic rings depends on the nature of interaction of quinoline with the metal center in the catalyst.[17,18] The observed exclusive selectivity could be explained on the basis of quinoline interaction with or its absorption to the active metal through nitrogen in the ring, which can impact the instantaneous microenvironment generated around the metal center.[53] This results in strong interaction by virtue of the basic nature of the support which plays a crucial role in directing the reaction.[54]

Hydrogenation of *N*-heterocycles using gaseous H_2 pressure

The catalytic performance of Rh@Fe_3O_4 catalyst towards the hydrogenation of a series of *N*-heterocyclic compounds with gaseous H_2 was evaluated in water, methanol, IPA, toluene and THF as well as without a medium. The reaction variables and the results are summarized in Table 3. First, the reactions were optimized using quinoline as model substrate with the variation of solvent, pressure and temperatures. Here, influence of solvent was clear. Quinoline (0.5 mmol) is hydrogenated in 2 h to py-THQ in water under 20 bar hydrogen pressure. While employing other solvents like toluene and methanol, there were significant drop on conversion (table 3, entry# 2 and 3). The same reaction was tried at room temperature and ended up with no conversion (table 3, entry#1). But on increasing temperature at 50 °C, the conversion was quantitative with maximum selectivity.

The effect of pressure on the conversion and selectivity were studied and summarized. In case of pyridine, the complete hydrogenation occurred in 10 h at 115 °C without solvent; a similar trend was seen for pyrazine hydrogenation in IPA (table 3, entry# 4 and 5). The hydrogenation activity of the catalyst was also evaluated for the five-membered ring heterocycles (table 3, entry# 6-7). At 130 °C/40 bar, indole hydrogenation attained 70% conversion with 100% selectivity after 24 h in THF (table 3, entry# 6). However, only 12% conversion was achieved at 150 °C/40 bar, in the case of 2-methyl indole, even after 24 h of reaction time (table 3, entry# 7). This anomaly could be partly ascribed to the steric hindrance of the methyl group and the lone pair on the nitrogen atom in the ring.

The influence of the basic support on quinoline hydrogenation were studied using series of metal oxides such as MgO, CaO, as well as the support used in this work, Fe_3O_4. It was observed that as the basic nature of the support increased (Fe_3O_4 < MgO < CaO) the rate of hydrogenation become faster and this was reflected from its TOF values in table 3 (entries# 10, and 11).[54] This observation can be explained that the hydroxylated basic supports, such as CaO, MgO and Fe_3O_4 have been shown to be capable of engaging the *N*-bearing heterocyclic moieties via hydrogen bonding.[55-57]

Aromatic hydrogenation

Hydrogenation of simple aromatics, like benzene, toluene,

Table 3. Rh@Fe_3O_4-mediated hydrogenation of *N*-heteroarene by gaseous H_2

Entry	Subst.[a]	Prod.	Solv.	Time (h)	Temp (°C)	Pres. (bar)	Conv.[b] (%)	Sel.[c] (%)	TOF (h^{-1})
1			Water	2 2 2	rt 40 50	20 20 20	--- >67 >99	--- 100 100	--- --- 54
2			Methanol	2	50	30	61	100	33
3			Toluene	2	50	30	36	100	19
4[d]			None	10	115	40	>99	100	217
5[e]			IPA	14	130	30	>99	100	93
6			THF	24	140	40	70	100	3
7			THF	24	150	40	12	100	0.5
8[f]			Water	2	50	20	<4	nd	nd
9[g]			water	2	50	20	<2	nd	nd
10[h]			Water	1.5	50	20	98	100	71
11[i]			Water	1	50	20	>99	100	108

5 mg catalyst used; TOF value was based on mole of product produced with the mole of Rh in the Rh@Fe_3O_4 per hour; [a]amount of substrate used 0.5 mmol; [b]measured by GC; [c]identified by GC-MS and NMR; [d]substrate used 12 mmol, 1mL; [e]substrate used 6 mmol; [f]without catalyst, Rh@Fe_3O_4; [g]with Fe_3O_4 only; [h]MgO as support; [i]CaO as support; nd: not determined.

xylene etc, was performed with gaseous H_2 pressure without

any solvent. Here we realized that the reaction temperature is one of the important determining factor to produce the desired hydrogenated compound. For instance, it was noticed that benzene could be rapidly hydrogenated to cyclohexane at 100 °C and 30 bar pressure (table 4, entry # 1). In case of toluene, hydrogenation into methylcyclohexane, 51% conversion was achieved at 115 °C at 50 bar pressure and this increased to 70% when temperature was raised to 130 °C for

Table 4. Rh@Fe_3O_4-mediated hydrogenation[a] of aromatic compounds by gaseous H_2 without a solvent

Entry	Substrate	Prod.	Time (h)	Temp. (°C)	Pres. (bar)	Conv.[b] (%)	Sel.[c] (%)	TOF (h^{-1})
1[d]			8	100	30	>99	100	297
2[e]			24 24	115 130	50 50	51 70	100 100	21 29
3[e]	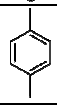	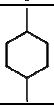	24	150	50	22	100	8

[a] 5 mg catalyst used for all above reaction; [b]measured by GC; [c]identified by GC-MS; [d]used 1 mL benzene; [e]used 0.5 mL toluene and *p*-xylene

View Article Online
DOI: 10.1039/C8CY00936H

the same reaction time of 24 h. This activity enhancement also implies catalyst stability at higher temperature. In the case of other arenes, the hydrogenation propensity decreased steadily with the increase of methyl substitution (table 4, entry#3). For example, p-xylene could be hydrogenated to give 1,4-dimethyl cyclohexane with 22% of conversion at 50 bar pressure.

Isotope labelling and mechanism elucidation

Based on the observed activity and selectivity of the catalyst, a reaction route is proposed (Scheme 1). For this, isotope labelling studies were performed by using D_2O instead of H_2O, as the reaction medium and identifying the location of additional hydrogen in the hydrogenated quinoline.

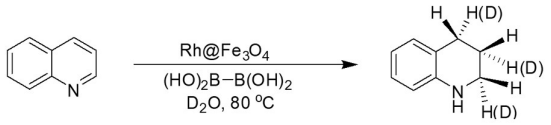

Scheme 1. Isotopic labelling experiment

Mass spectrometric and NMR spectroscopic studies revealed the possible deuteration sites of quinoline which was estimated to be deuterated at the C(2), C(3) and C(4) positions of the *N*-bearing heterocyclic ring. Likewise, nitrogen should also be deuterated. However, the possibility of rapid exchange of deuterium with hydrogen coming from trace moisture during the workup process, mitigates the deuteration of nitrogen (*see supporting information, Fig S8, S9 and S15*).[58]

From the above discussion, it is evident that quinoline can be quantitatively and selectively reduced to py-THQ in water by THDB. The results also highlight the definite role of water molecules in the hydrogenation process. On the basis of above discussion, we propose the catalytic cycle for the hydrogenation of quinoline in the following sequence (Scheme 2).

Firstly, Rh undergoes oxidative addition to give **1**, followed by the coordination of water molecule to boron atom to form the adduct **2**. The Rh- hydride complex **3** is produced by the elimination of boric acid (H_3BO_3). This leads quinoline which is in intimate interaction with the magnetite support through hydrogen bonding, to enter into the catalytic cycle and generate an intermediate **4**. At this point, the C(2)-N bond is reduced by the transfer of hydrogen from Rh-hydride **3** in to C(2) as it is the most electrophilic site in quinoline.[59] Since there could be an inherent difficulty for the nitrogen atom to disrupt its aromaticity in the heterocyclic ring,[60] this could be the rate determining step. Coordination of another water molecule with boron atom generates another Rh-hydride complex **5**, followed by another hydrogen transfer (and liberating boric acid) gives **6**. Reductive elimination then occurs to produce an intermediate compound, 1,2-dihydroquinoline (**7**). Same sequence of process occurs at positions C(3) and C(4), leading to the formation of the ultimate product, viz, 1,2,3,4-tetrahydroquinoline. As can be readily seen from the proposed catalytic reaction scheme, at least four equivalent of

Scheme 2. Proposed catalytic cycle for hydrogenation of quinoline in water with THDB

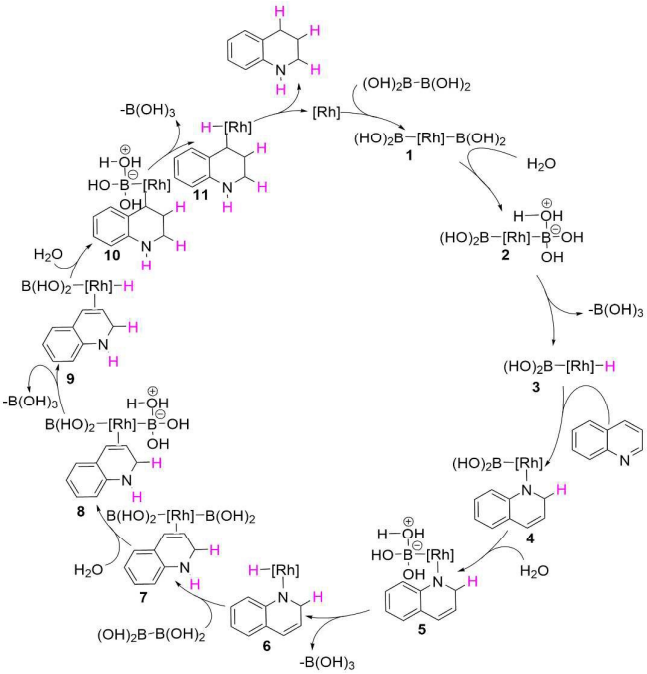

water molecules are required for the hydrogenation of one molecule of quinoline, producing py-THQ.

Re-usability studies

To assess the reusability of the spent catalyst in subsequent hydrogenation cycles of quinoline in aqueous medium under optimized reaction condition, it was isolated from the product by putting a magnet at the bottom of the flask and decanting the liquid. The catalyst was thoroughly washed several times with methanol and dichloromethane, and dried for use in the next hydrogenation step without adding any fresh material. This procedure was repeated several times. It was found that the catalyst could be used in 16 consecutive cycles, showing excellent catalytic propensity. However, the efficiency in terms of catalytic activity declined slightly with increasing number of cycles; it was ~93% by the 16th cycle (Figure 5b), which could be compensated by increasing the on-stream reaction time.

The spent catalyst was collected at the end of cumulative cycles and its metal contents quantified by ICP-OES which showed 6.1% loss of Rh as a result of leaching from the surface of magnetic nanoparticles and may be this slight amount of loss of Rh was associated with the exhaustion of the catalyst. The stability of the catalyst corroborated by the HRTEM and

View Article Online
DOI: 10.1039/C8CY00936H

STEM investigations on the recycled catalyst, which showed no severe damage to the magnetite surface; no sign of surface agglomeration was observed either (*see supporting information*, Fig S2).

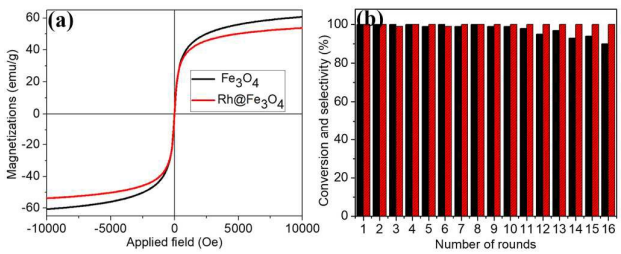

Fig. 5 (a) Magnetic hysteresis loops of $Rh@Fe_3O_4$ at room temperature with 1 tesla magnet (b) re-suability of the catalyst for quinoline hydrogenation at 50 °C under molecular H_2 pressure in water (■ conversion and ■ selectivity).

Conclusions

This study demonstrated a path to facile synthesis of sub-nano sized Rh particles supported on superparamagnetic iron oxide nanoparticles (SPIONs, Fe_3O_4), for efficient hydrogenation and of a series of *N*-bearing heterocyclic and other aromatic compounds under mild experimental conditions in water. For the first time, the chemoselective hydrogenation of quinoline in water carried out using THDB and achieved excellent conversion and selectivity with the very short span of time (10 min.). The Rh@ Fe_3O_4 construct was a stable and versatile catalyst in the hydrogenation of other heterocycles, such as, pyridine, pyrazine and indole, and, some simple aromatic compounds, such as, benzene, toluene and xylene, with gaseous hydrogen under moderate pressure and temperature. Isotopic labelling studies was successfully revealed the source of hydrogen and the role of THDB in the reaction. A mechanism of hydrogen transfer reaction of quinoline was proposed. The catalyst was shown to possess remarkable reactivity towards hydrogenation reaction for 16 consecutive cycles. The combination of water and tetrahydroxydiboron as hydrogenation precursor offers an environmentally benign synthesis strategy for industrial relevant compounds. Work on the catalytic transformation reaction of other organic functional groups is currently under investigation in our laboratory.

Acknowledgments

MNS gratefully acknowledges the Center of Research Excellence in Nanotechnology (CENT) for its generous supports and internal funding under the project code # NT-2015-MNS-01 and NT-2018-MNS.

Conflicts of interest

There are no conflicts to declare.

Notes and references

1. Z. Zhang, N. A. Butt and W. Zhang, *Chem. Rev.*, 2016, **116**, 14769–14827.
2. P. Etayoa and A. Vidal-Ferran, *Chem. Soc. Rev.*, 2013, **42**, 728-754.
3. Y. Hao, X. Jiao, H. Zou, H. Yang and Jian Liu, *J. Mater. Chem. A*, 2017, **5**, 16162-16170.
4. T. Zell and D. Milstein, *Acc. Chem. Res.*, 2015, **48**, 1979–1994.
5. O. Saidi and J. M. J. Williams, *Top. Organomet. Chem.*, 2011, **34**, 77–106.
6. A. Fabrello, A. Bachelier, M. Urrutigoïty and P. Kalck, *Coord. Chem. Rev.*, 2010, **254**, 273–287.
7. P. Zhao, X. Feng, D. Huang, G. Yang and D. Astruc, *Coord. Chem. Rev.*, 2015, **287**, 114–136.
8. J. Liang, X. Zhang, L. Jing and H. Yang, *Chin. J. Catal.*, 2017, **38**, 1252–1260.
9. J. Huang, F. Cheng, B. P. Binks and H. Yang, *J. Am. Chem. Soc.* 2015, **137**, 15015–15025.
10. V. Sridharan, P. A. Suryavanshi and J. C. Menendez, *Chem. Rev.,* 2011, **111**, 7157–7259.
11. D. S. Wang, Q. A. Chen, S. M. Lu and Y. G. Zhou, *Chem. Rev.,* 2012, **112**, 2557-2590.
12. E. Baralt, S. J. Smith, J. Hurwitz, I. T. Horvath and R. H. Fish, *J. Am. Chem. Soc.*, 1992, **114**, 5187-5196.
13. H. Konnerth and M. H. G. Prechtl, *Green Chem.*, 2017, **19**, 2762-2767.
14. J. Wen, R. Tan, S. Liu, Q. Zhao and X. Zhang, *Chem. Sci.*, 2016, **7**, 3047-3051.
15. X. C. Zhang, Y. H. Hu, C. F. Chen, Q. Fang, L. Y. Yang, Y. B. Lu, L. J. Xie, J. Wu, S. Li and W. Fang, *Chem. Sci.*, 2016, **7**, 4594-4599.
16. Y. T. Xia, J. Ma, X. D. Wang, L. Yanga and L. Wu, *Catal. Sci. Technol.*, 2017, **7**, 5515-5520.
17. R. H. Fish, E. Baralt and S. J. Smith, *Organometallics*, 1991, **10**, 54-56.
18. R. H. Fish, A. D. Thormodsen, R. S Moore, D. L Perry and H. Heinemann, *J. Catal.*, 1986, **102**, 270-273.
19. R. H. Fish, J. L. Tan and A. D. Thormodsen, *J. Org. Chem.*, 1984, **49**, 4500-4505.
20. N. Mrsaic, L. Lefort, J. A. F. Boogers, A. J. Minnaard, B. L. Feringa and J.G. de Vries, *Adv. Synth. Catal.,* 2008, **350**, 1081 – 1089.
21. R. Abu-Reziq, H. Alper, D. Wang and M. L. Post, *J. Am. Chem. Soc.*, 2006, **128**, 5279-5282.
22. Rahi, M. Fang, A. Ahmed and R. A. Sánchez-Delgado, *Dalton Trans.,* 2012, **41**, 14490–14497.
23. V. Polshettiwar and R. S. Varma, *Green Chem.*, 2010, **12**, 743-754.
24. F. Nador, Y. Moglie, C. Vitale, M. Yus, F. Alonso and G. Radivoy, *Tetrahedron,* 2010, **66**, 4318-4325.
25. G. Radivoy, F. Alonso and M. Yus, *Tetrahedron,* 1999, **55**, 14479-14490.
26. M. Fang and R. A. Sanchez-Delgado, *J. Catal.*, 2014, **311**, 357–368.
27. L. Zhang, X. Wang, Y. Xue, X. Zeng, H. Chen, R. Li and S. Wang, *Catal. Sci. Technol.*, 2014, **4**, 1939–1948.

View Article Online
DOI: 10.1039/C8CY00936H

28. D. Zhu, H. Jiang, L. Zhang, X. Zheng, H. Fu, M. Yuan, H. Chen and R. Li, *ChemCatChem*, 2014, **6**, 2954–2960.
29. M. Niu, Y. Wang, P. Chen, D. Du, J. Jiang and Z, Jin, *Catal. Sci. Technol.*, 2015, **5**, 4746–4749.
30. G. Y. Fan and J. Wu, *Catal. Commun.*, 2013, **31**, 81–85.
31. M. Campanati, M. Casagrande, I. Fagiolino, M. Lenarda, L. Storaro, M. Battagliarin and A. Vaccari, *J. Mol. Catal. A*, 2002, **184**, 267.
32. A. Karakulina, A. Gopakumar, I. AkÅok, B. L. Roulier, T. La Grange, S. A. Katsyuba, S. Das and P. J. Dyson, *Angew. Chem. Int. Ed.,* 2016, **55**, 292 –296.
33. P. Barbaro, L. Gonsalvi, A. Guerriero and F. Liguori, *Green Chem.,* 2012, **14**, 3211–3219.
34. D. Ge, L. Hu, J. Wang, X. Li, F. Qi, J. Lu, X. Cao and H. Gu, *ChemCatChem*, 2013, **5**, 2183–2186.
35. M. M. Dell'Anna, V. F. Capodiferro, M. Mali, D. Manno, P. Cotugno, A. Monopoli and P. Mastrorilli, *Appl. Catal. A,* 2014, **481**, 89–95.
36. Y. Gong, P. Zhang, X. Xu, Y. Li, H. Li and Y. Wang, *J. Catal.,* 2013, **297**, 272–280.
37. M. Guo, C. Li and Q. Yang, *Catal. Sci. Technol.*, 2017, **7**, 2221-2228.
38. L. Tao, Q. Zhang, S.-S. Li, X. Liu, Y. M. Liu and Y. Cao, *Adv. Synth. Catal.*, 2015, **357**, 753–760.
39. M. Yan, T. Jin, Q. Chen, H. E. Ho, T. Fujita, L. Y. Chen, M. Bao, M. W. Chen, N. Asao and Y. Yamamoto, *Org. Lett.*, 2013, **15**, 1484–1487.
40. A. R. McDonald, C. Muller, D. Vogt, G. P. M. van Klink and G. van Koten, *Green Chem.*, 2008, **10**, 424–432.
41. J. Wang, B. Xu, H. Sun and G. Song, *Tetrahedron Lett.*, 2013, **54**, 238–241.
42. Y. Zhu, S. C. Peng, A. Emi, S. Zhenshun, Monalisa and R. A. Kemp, *Adv. Synth. Catal.*, 2007, **349**, 1917–1922.
43. Sh. Li, F. Chen, N. Li, W. Wang, X. Sheng, A. Wang, Y. Cong, X. Wang, and T. Zhang, *ChemSusChem*, 2017, **10**, 711 – 719.
44. S. Tang, L. Wang, Y. Zhang, S. Li, S. Tian and B. Wang, *Fuel Process. Technol.*, 2012, **95**, 84–89.
45. M. N. Shaikh, M. Bououdina, A. A. Jimoh, M. A. Aziz, A. Helal, A. S. Hakeem, Z. H. Yamani and T.-J. Kim, *New J. Chem.*, 2015, **39**, 7293-7299.
46. M. N. Shaikh, M. A. Aziz, A. Helal, M. Bououdina, Z. H. Yamani and T.-J. Kim, *RSC Adv.*, 2016, **6**, 41687-41695.
47. R. S. Varma, *Pure Appl. Chem.*, 2013, **85**, 1703-1709.
48. C. Deraedt, R. Ye, W. T. Ralston, F. D. Toste and G. A. Somorjai, *J. Am. Chem. Soc.*, 2017, **139**, 18084–18092.
49. N. Pinna, S. Grancharov, P. Beato, P. Bonville, M. Antonietti and M. Niederberger, *Chem. Mater.*, 2005, **17**, 3044-3049.
50. T. Yang, X.-D. Wen, J. Ren, Y.-W. Li and J.-G. Wang, *J. Fuel Chem. &Tech.*, 2010, **38**, 121-128.
51. C.-H. Pélisson, D.-N. Audrey and A. Roucou, *ACS Sustainable Chem. Eng.,* 2016, **4**, 1834–1839.
52. Y. Zhang, M. E. Grass, S. E. Habas, F. Tao, T. Zhang, P. Yang and G. A. Somorjai, *J. Phys. Chem. C,* 2007, ***111***, 12243-12253.
53. M. Koneracka, P. Kopcansky, M. Antalmk, M. Timko, C. N. Ramchand, D. Lobo, R. V. Mehta and R. V. Upadhyay, *J. Magn. Magn. Mater.*, 1999, **201**, 427-432.
54. A. Sánchez, M. Fang, A. Ahmed and R. A. Sánchez-Delgado, *Applied Catalysis A: General*, 2014, **477**, 117–124.
55. L. Bai, X. Wang, Q. Chen, Y. Ye, H. Zheng, J. Guo, Y. Yin and C. Gao, *Angew. Chem., Int. Ed.,* 2016, **55**, 15656–15661.
56. H. Mao, C. Chen, X. Liao and B. Shi, *J. Mol. Catal. A: Chem.,* 2011, **341**, 51–56.
57. M. M. Dell'Anna, G. Romanazzia, S. Intini, A. Rizzutia, C. Leonellib, A. F.Piccinnia and P. Mastrorilli, *J. Mol. Catal A: Chem.,* 2015, **402**, 83–91.
58. G. Eros, K. Nagy, H. Mehdi, I. Papai, P. Nagy, P. Kiraly, G. Tarkanyi and T. Soos, *Chem. Eur. J.,* 2012, **18**, 574 – 585.
59. M. Rosales, Y. Alvarado, M. Boves, R. Rubio, H. Soscun and R. SaÂnchez-Delgado, *Transition Met. Chem.,* 1995, **20**, 246-251.
60. C. Bianchini, P. Barbaro, M. Macchi, A. Meli and F. Vizza, *Helv. Chim. Acta*, 2001, **84**, 2895-2923.

View Article Online
DOI: 10.1039/C8CY00936H

Graphical abstract

Facile hydrogenation of *N*-heteroarenes by magnetic nanoparticles supported sub-nanometric Rh catalysts in aqueous medium

This work describes the preparation and systematic characterization of reusable magnetic heterogeneous nanocatalyst (Rh@Fe_3O_4) for the hydrogenation of N-heterocycles and simple aromatics. The activity, selectivity and mechanistic catalytic pathway were investigated.